(2+1)-dimensional soliton formation in photorefractive $Bi_{12}SiO_{20}$ crystals

E. Fazio, W. Ramadan,* A. Belardini, A. Bosco, and M. Bertolotti
Università degli Studi di Roma "La Sapienza" and INFM Dipartimento di Energetica, via Scarpa 16, I-00161 Roma, Italy

A. Petris and V. I. Vlad
Institute of Atomic Physics, National Institute of Lasers, Plasma and Radiation Physics, and The Romanian Academy—Center of Advanced Studies in Physics, Atomistii 111, R-76900 Bucharest, Romania

(Received 24 May 2002; revised manuscript received 8 October 2002; published 26 February 2003)

(2+1)-dimensional spatial solitons in $Bi_{12}SiO_{20}$ (BSO) photorefractive crystals with large optical activity are experimentally demonstrated. The soliton formation when a Gaussian beam is injected at the input has been previously analyzed numerically and then experimentally investigated. We demonstrate analytically, numerically, and experimentally that by applying static electric biases of high values, the polarization rotation accelerates: this acceleration prevents the beam from broadening if the polarization rotation period becomes shorter than the diffraction length. Contemporary to this nonlinear optical activity, an induced birefringence affects the beam polarization state. Analysis of the polarization dynamics shows that the polarization changes nonuniformly across the beam (with a field dependent speed) until about 30–35 kV/cm; above this limit, the whole beam has just one polarization state. Representation on the Poincaré sphere of the polarization dynamics reveals the existence of a stable polarization trajectory closed around a polarization attractor that depends on the linear optical activity and on the photorefractive nonlinearity. The experimental soliton is well described by the analytical solutions already obtained [Fazio *et al.*, Phys. Rev. E **66**, 016605 (2002)].

DOI: 10.1103/PhysRevE.67.026611 PACS number(s): 42.65.Tg

I. INTRODUCTION

Spatial solitons in photorefractive materials have been predicted in 1992 [1] and observed in 1993 [2]. Since then, many papers on solitons in photorefractive crystals have been published: a complete review on this can be found in the book by DelRe, Grosignani, and Porto [3].

Optical activity has been considered in the past as a detrimental factor for photorefractive spatial solitons formation [4,5]. Photorefractive materials need a static electric field of bias, orthogonal to the light polarization in order to induce optical nonlinearity and, as a consequence, to generate spatial solitons [6]. The optical activity rotates the polarization plane of the optical field, and superimposes it periodically along the crystallographic direction without optical nonlinearity, leading to the loss of soliton confinement (diffraction). Competition between self-focusing, experienced for some orientations of polarization, and diffraction governs the beam dynamics.

In materials with low optical activity, as for example, for $Bi_{12}TiO_{12}$ (BTO) (with a rotatory power of about 8°–10° mm^{-1} at 633 nm [3]), this obstacle was overpassed limiting the propagation length and, consequently, limiting the rotation around the polarization direction subjected to self-focusing. This procedure, however, cannot be followed for materials with strong optical activity, as for example for BSO crystal; in this case, the polarization vector rotates by about 39°/mm at 514 nm or 45°/mm at 488 nm [7,8] (just to mention some wavelengths useful for the photorefractive properties), and the crystal should be very short to limit the polarization rotation. In this case, it is difficult to ensure the nonlinear effect (confinement) along reasonable propagation distances. Recently, the possibility of breathing solitonlike propagation in such materials has been analytically demonstrated [9].

In the present paper, we report the experimental observation of (2+1)-dimensional spatial soliton propagation in BSO crystals. We shall demonstrate that solitonic beams are always possible in photorefractive crystals with large optical activity, for any crystallographic direction of the bias field, for very high static bias fields. In fact, by increasing the static bias field, the polarization rotation along the propagation direction accelerates: the rotation period in these regimes can be much shorter than the diffraction length, preventing for efficient diffraction of the beam. We shall analytically demonstrate that the angular speed is inversely proportional to the light beam intensity: thus a competition between acceleration (given by the static field) and deceleration (given by the beam intensity) stabilizes the rotation speed which remains constant across the beam profile. In this case, the beam angular momentum remains constant along the whole propagation, accelerating and decelerating the polarization according to the breathing of the transversal dimension. However, it was already demonstrated [10,11] that the photorefractive nonlinearity generated also an effective birefringence, which modifies the polarization state from the linear to the elliptical regime. We shall consider here the induced birefringence and demonstrate that the soliton regime has a well defined stable polarization state, acting as an attractor for the polarization dynamics when a Gaussian beam is injected at the input.

II. DYNAMICS OF THE SOLITON FORMATION

In order to characterize the whole process of the soliton formation, from the self-focusing to the solitonic regime, nu-

*On leave from Faculty of Sciences, University of Mansoura, Damietta, Egypt.

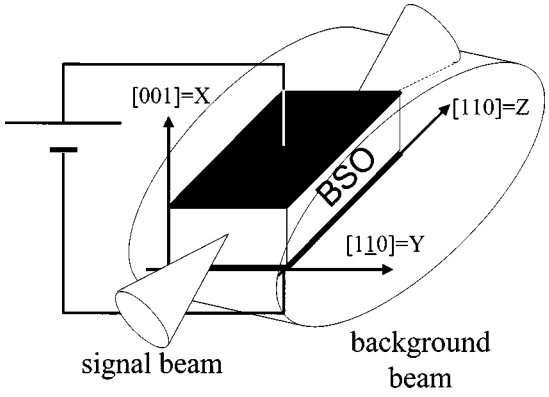

FIG. 1. Experimental crystal orientations: the BSO crystal was 8 mm long in its [110] crystallographic direction (called *Z*), 2 mm along [001] (called *X*), and 3 mm along [$1\bar{1}0$] called *Y*. The external bias was applied along *X*; a background beam, incoherent to the signal beam, was sent along *Y* and the signal propagated along *Z*.

merical simulations of light propagation have been performed. For this purpose, we have considered (see Fig. 1) a BSO crystal biased along its [001] crystallographic direction (*X*) by a static high voltage field, and contemporarily illuminated along the [$1\bar{1}0$] crystallographic direction (*Y*) by an incoherent background beam. A second beam (called signal or soliton beam) was injected along the [110] crystallographic direction (*Z*) in order to form a soliton. Following this configuration, the electric field of the signal beam has two components, one along *X* and *Y*, respectively; their propagations are described by two equations, coupled together through the optical activity (Γ term) and the photorefractive nonlinearity $\delta\varepsilon_{\mathrm{NL}}$:

$$\left(2ik\frac{\partial}{\partial z}+\nabla^2_{\mathrm{transv}}\right)E_x-i\Gamma E_y=0,$$
$$\left(2ik\frac{\partial}{\partial z}+\nabla^2_{\mathrm{transv}}+\delta\varepsilon_{\mathrm{NL}}\right)E_y+i\Gamma E_x=0. \quad (1)$$

The optical activity term here is represented by the gyration constant Γ, defined as the ratio $\Gamma=2\rho_0/k$ between the linear rotatory power ρ_0 and the light wave number k inside the crystal. For a BSO crystal, ρ_0 is about 39° mm^{-1} at the operating wavelength of 514 nm. The photorefractive nonlinear dielectric constant $\delta\varepsilon_{\mathrm{NL}}$ was previously described by Crosignani *et al.* [12]; in the steady state and drift dominated transport conditions, it can be approximated as

$$\delta\varepsilon_{\mathrm{NL}}=-kn_0^2r_{41}E_{\mathrm{sc}}=-kn_0^2r_{41}\frac{E_{\mathrm{bias}}}{1+I_{\mathrm{soliton}}/I_{\mathrm{background}}}, \quad (2)$$

where n_0 is the linear refractive index, r_{41} is the electro-optic coefficient, and E_{sc} is the electric field that screens the applied static bias E_{bias}; the screening field is a function of the applied bias and of the intensity ratio between the soliton (I_{soliton}) and the background beams ($I_{\mathrm{background}}$), respectively.

Please note that Eq. (2), used to simulate soliton formation, is mainly valid in one-dimensional (1D) case. The correct 2D model should involve the material dynamics [13]. However, the used model still well describes the experimental results in this special case, different from that published by anyone before, where a really high bias field is applied. Anyhow, the full material dynamics might give further information on asymmetries that could appear on the beam shape.

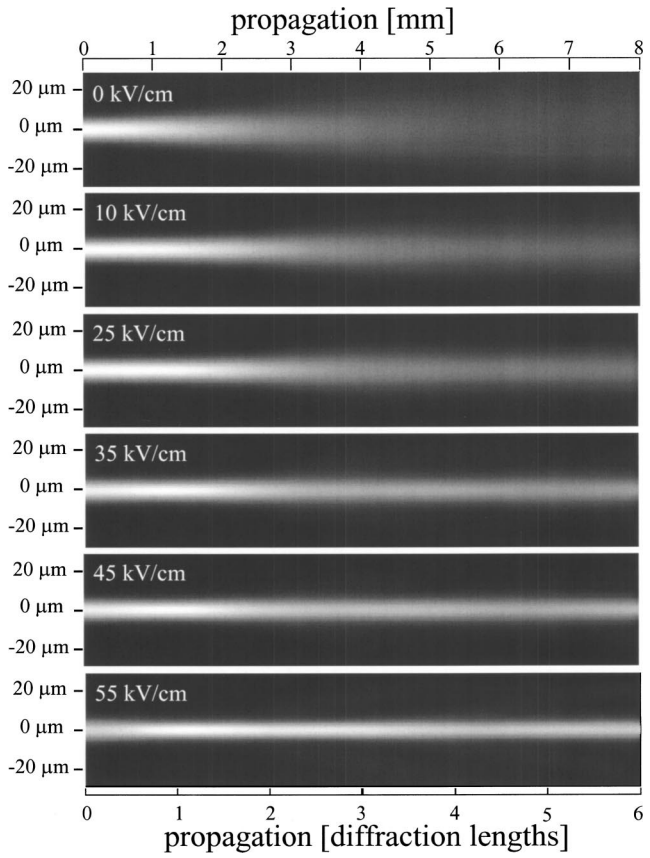

FIG. 2. Numerical solutions of the beam propagation for different biases. At 0 kV/cm, the beam linearly diffracts. Increasing the applied bias the beam experiences self-focusing more and more efficient: however, only at about 55 kV/cm, the propagation is keeping the same shape along the whole 8-mm propagation, which corresponds to six diffraction lengths.

Numerical integrations of Eqs. (1) consider a Gaussian beam injected at the input, as large as about 10 μm which propagates for 8 mm within the crystal (which corresponds to about 5.5–6.0 diffraction lengths).

Without external bias the laser beam just diffracts, as shown in Fig. 2(a). Applying an increasing bias field, the laser beam is more and more confined, but only above 45 kV/cm diffraction is completely compensated [see Figs. 2(b)–2(f)]. These results were obtained injecting a beam with a linear polarization along *Y*: in fact, we have found that the injected polarization state is critical for the soliton formation. In Fig. 3, we report on a comparison of beam propagation at the same bias conditions of 55 kV/cm, but starting from different polarization states (which are represented on the left-hand side as thicker lines; the optical activity rotation direction is reported as circular arrows for completeness).

Injecting an *X*-polarization state [Fig. 3(a)] i.e., with the wave-electric field parallel to the external bias, the beam

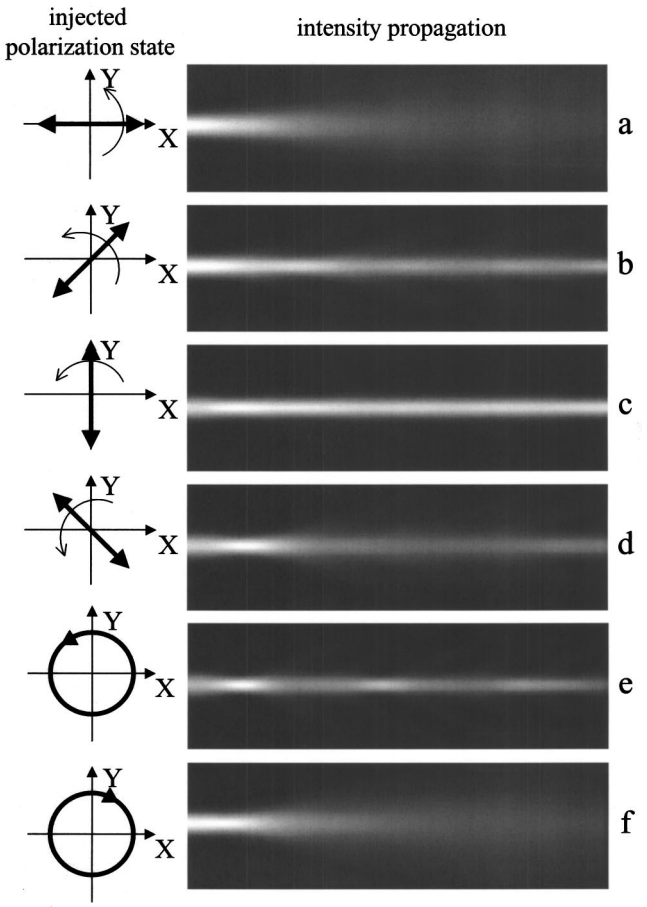

FIG. 3. Numerical solutions of the beam propagation at 55 kV/cm of external bias for different input polarization states. On the left-hand side, the input polarization states are represented as thick arrows together with second thin and round arrow that gives the optical activity rotation axis. Injecting an *X* polarized beam (a), the beam is not confined but diffracts; if instead an *Y* polarized beam is injected (c), the beam is indeed self-focused and a soliton is formed. Injecting still linear polarizations at 45° (b) and 135° (d), the beams are still confined, but strong breathings influence their propagations, as also occurring is an injected circular polarization that is rotating in the same axis of the optical activity (e). If there is still a circular polarization but with antiparallel rotation with respect to the optical activity injected (f), the beam is not confined and diffracts.

does not compensate diffraction and diverges. In fact, only the *Y* component experiences self-focusing [see Eq. (1)]. If the input polarization is along the *Y* direction [Fig. 3(c)], the beam is indeed self-trapped because now the photorefractive nonlinearity is efficient from the beginning. The two intermediate conditions, i.e., polarization states at 45° [Fig. 3(b)] and 135° [Fig. 3(d)], respectively, give again a self-trapping of the beam, but this time with different efficiencies according to the rotation given by the optical activity (if the polarization is driven towards or away from the *Y* direction). For circularly polarized beams, the rotation direction must be considered with respect to the optical activity one: in Figs. 3(e),3(f), polarization rotations parallel and antiparallel to the optical activity are reported, respectively. In the former case (parallel), a self-trapped beam is formed (even if a strong

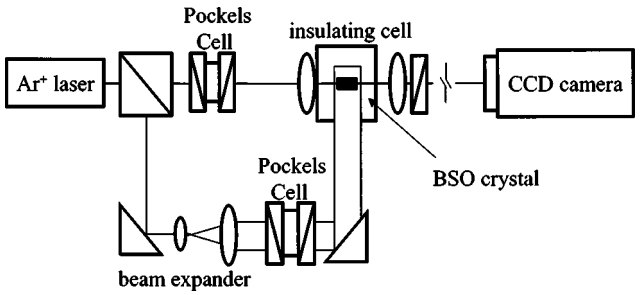

FIG. 4. Experimental setup used to investigate the soliton formation. The laser beam from an Ar laser was divided in two beams, one for the background and one for the signal. The background was made incoherent (with a delay line longer than the coherent length of the laser) enlarged and sent transversally on the sample. It was kept within an insulating cell to avoid electric discharge. The output face of the crystal was imaged on a CCD by using an optical system with magnification. The images were then recorded by a PC.

breathing is excited), while in the latter (antiparallel one), the beam is diverging.

We have experimentally tested the beam self-trapping and soliton formation by using the setup shown in Fig. 4. Light from an Ar^+ laser at 514.5 nm was used for both the signal beam and the incoherent background. Two Pockels cells, one for the background and one for the signal, respectively, set the light intensity and polarization state. The BSO crystal was 8 mm long along [110], 3 mm along $[1\bar{1}0]$, and 2 mm along [001]; the external static bias was applied along [001]. In order to avoid electric discharge between electrodes, the sample was kept within an insulating cell. The signal beam (*Y* polarized) was focused down to a waist of 10 μm and propagated within the sample for about six diffraction lengths. At the crystal output plane, it was imaged on a charge-coupled device (CCD) camera by an optical system with a magnification of 43.

Images of the beam at the input and at output planes have been recorded for bias fields ranging from 0 up to about 55 kV/cm, as shown in Fig. 5. Applying an increasing bias field, the light beam becomes narrower and narrower. At 45 and 55 kV/cm, the diffraction is almost completely compensated. In Fig. 6, the output waist dimensions in the two *X* and *Y* directions, respectively, normalized to the input one, are reported as a function of the applied bias. The beam shrinkage shows a saturating trend, down to a beam dimension of the same order of the input beam. The shrinkage trend is different for the two transverse coordinates: the obtained soliton-like beam is not circular but elliptical, with an ellipticity factor (defined as the ratio of the minimum axis to maximum axis) of about 60%. This is a consequence of the anisotropy of the screening process [14].

III. POLARIZATION DYNAMICS

How is it possible that a light beam can compensate diffraction, if its polarization is periodically rotated along a direction without self-focusing? If the rotation is weak, the propagation does not modify significantly the polarization state, and diffraction can be compensated (this is the case of

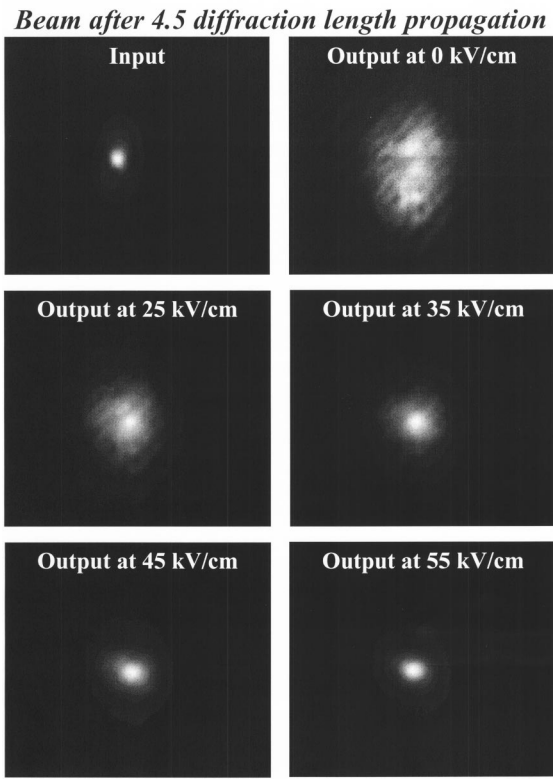

FIG. 5. Experimental images of the output beam increasing the bias field applied. A comparison with the input beam demonstrates that at about 55 kV/cm, the diffraction is almost completely compensated.

other photorefractive crystals with lower optical activity, as for example, BTO for which the polarization rotates for few degrees for each millimeter of propagation). Larger rotations can indeed cause some problems if their period is comparable to the diffraction length. In this case, the rotation keeps the polarization for a long propagation in the diffracting state, and consequently the beam diverges. However, really high optical activity could produce rotation periods much shorter than the diffraction length. This case is now again favorable to the soliton formation, because the diffracting state in this case is kept for a short propagation, not enough to make the beam diverge. However, this case of optical activity rotation period, which is much shorter than the diffraction length, is not our experimental case for the BSO crystal, for which one polarization component remains for about 4–5 mm before being completely converted into the other one, and the beam diffraction length is about 1.8 mm. If this is true in the linear case or for relatively low applied biases, it is not valid anymore for really high biases, for which the polarization rotation speed can accelerate many times because of the photorefractive nonlinearity.

Let us consider the experimental conditions described in Fig. 1, i.e., a static bias along the Y direction and a signal beam propagating along the Z direction. For this particular orientation, the dielectric displacement vector $\vec{D}$ of the light should not have any component along the propagation direction Z: we can write without ambiguity $D_z = E_z = 0$. Then the

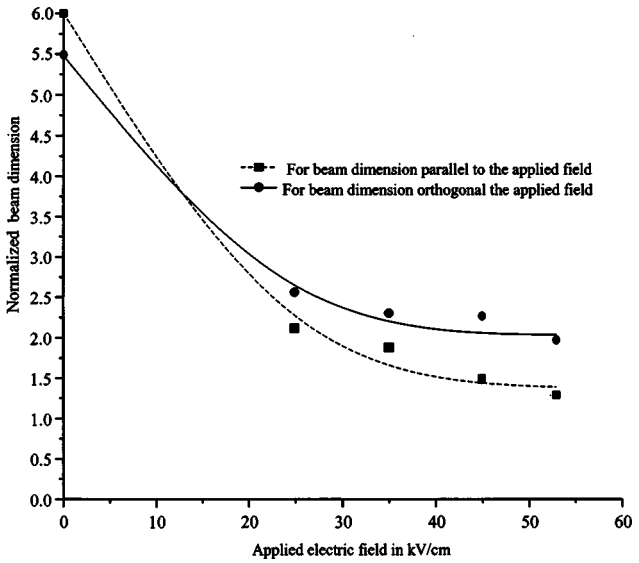

FIG. 6. Experimental beam dimensions along the X and Y directions for increasing biases. At about 50–55 kV/cm, the soliton is almost formed. The beam is not circular but elliptical, as a consequence of the asymmetrical action of the photorefractive nonlinearity on the two polarization components.

$\vec{E}$ vector lies in the plane generated by $\vec{D}$ and $\vec{k}$. From this hypothesis, we can write

$$\frac{D_x}{D_y} = \frac{E_x}{E_y}. \tag{3}$$

At the same time, the definition of the X and Y components of the $\vec{D}$ vector in the BSO photorefractive crystal gives

$$\begin{bmatrix} D_x \\ D_y \\ D_z \end{bmatrix} = \begin{bmatrix} n_0^2 & -i\Gamma & 0 \\ i\Gamma & n_0^2 + \dfrac{\delta\varepsilon_{\mathrm{NL}}}{k} & 0 \\ 0 & 0 & n_0^2 \end{bmatrix} \begin{bmatrix} E_x \\ E_y \\ E_z \end{bmatrix}. \tag{4}$$

Equations (3) and (4) must be simultaneously fulfilled; this leads to the definition of the whole beam as the superposition of two counter-rotating waves [15]: $E_y^{\pm} = iC^{\pm}E_x^{\pm}$, where $C^{\pm} = 1/(k_E \pm \sqrt{k_E^2+1})$ and $k_E = \delta\varepsilon_{\mathrm{NL}}/2\Gamma$. The overlapping of these two waves generates a field with rotating polarization if the waves have different propagation speeds. The speed difference is now described by the refractive index mismatch Δn of the two waves:

$$\Delta n = \frac{1}{2}(n_+ - n_-) = -\frac{\Gamma}{2n_0}\sqrt{1+k_E^2}. \tag{5}$$

Thus, defining the instantaneous polarization orientation of the rotating field as the angle $\alpha(z) = \Delta\vec{n}\cdot\vec{k}_0\hat{z}$, the instantaneous angular speed of the polarization rotation is

$$\rho(z) = \frac{\partial\alpha(z)}{\partial z} = \rho_0\sqrt{1+k_E^2}. \tag{6}$$

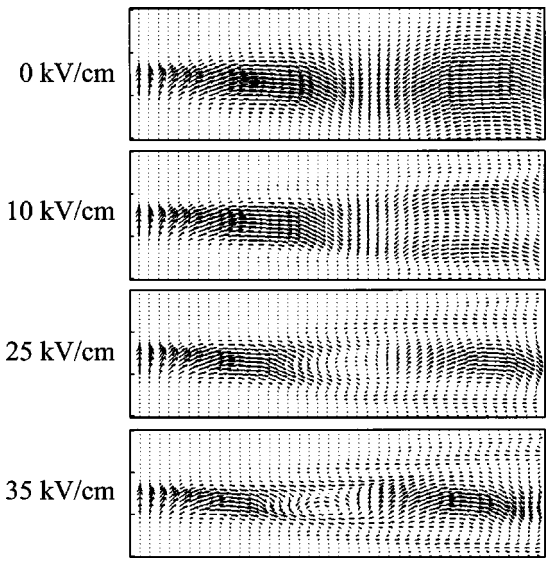

FIG. 7. Maps of the polarization orientation during the propagation. By increasing the bias field the polarization rotates faster, factor that helps the diffraction compensation. Some losses are present because of the self-focusing and of the beam breathing, which are caused by the injection of a Gaussian beam at the input. It is interesting to note that these losses have a fixed polarization that does not rotate any more. This map representation cannot be used anymore for applied biases higher than 35 kV/cm: in these cases, an induced birefringence modifies the polarization state from linear to elliptical. In this case, the polarization dynamics must be analyzed on a Poincaré sphere.

The factor $\sqrt{1+k_E^2}$ describes a correction to the linear rotation speed, which depends on the beam intensity, on its profile and on the external bias field intensity, through the k_E^2 term, i.e., through $\delta\varepsilon_{\mathrm{NL}}$. For the BSO crystals, at a bias of about 55 kV/cm with typical values of the intensity ratio lower than 1, $\rho=\rho_0\sqrt{1+k_E^2}\approx(3-4)\rho_0$: this acceleration of the polarization is not just a small correction. As a consequence, the rotation period can be three to four times shorter than in the linear case and, as a consequence, can become shorter than the diffraction length as well, compensating the diffraction.

We have calculated total conversion of the polarization state within 500–600 μm of propagation with about 40–50 kV/cm of bias. However, not only an acceleration of the optical activity influences the beam dynamics but also an induced birefringence: in fact, the asymmetric action of the photorefractive nonlinearity on the two light polarization components [see Eqs. (1)] produces an asymmetrical phase modulation of these components and consequently induces a nonlinear birefringence. This birefringence makes the polarization state to be no more linear but elliptical, with the major axis (which now coincides with the original linear polarization direction) rotating with the nonlinear speed $\rho(z)$ previously calculated. For bias fields lower than 20–25 kV/cm, the polarization ellipticity is not so large, and the induced birefringence can be considered as a small modification of a linear polarization state. For this reason, in Fig. 7 we have represented the maps of the polarization orientation during the beam propagation as arrows (but effectively the maps better represent the major axis orientations of elliptical polarization). Without external bias, a linear rotation of about $\frac{3}{2}\pi$ of the polarization occurs during the 8-mm propagation (more precisely the linear optical activity rotates the polarization plane for about 310°). Increasing the bias, the polarization starts to rotate faster: this acceleration is not uniform across the beam. It starts in one portion of the beam and then slowly widens across it. For higher biases, the induced birefringence can largely modify the polarization state until even circular polarizations are reached: in these regimes, the arrow mapping cannot be used any more because they lose significance. However, the polarization evolution during propagation can be still analyzed without ambiguity just by describing the polarization dynamics of the central portion of the beam on a Poincaré sphere. This is possible because we have observed that above 10–20 kV/cm of external bias, the polarization state is the same across all the transversal sections of the beam. This is a direct consequence of the saturating expression of the rotation speed $\rho(z)$: in fact, Eq. (6) states that $\rho(z)$ is directly proportional to k_E and consequently to the nonlinear dielectric constant $\delta\varepsilon_{\mathrm{NL}}$. This means that it is directly proportional to the external bias field as well [see Eq. (2)], and inversely proportional to the light beam intensity; then the rotation acceleration is favored by a high bias but it is slowed down in the center of the beam where the intensity is higher. The simultaneous combination of these two factors, larger and smaller accelerations across the beam, forces the polarization to reach just one constant and homogeneous state for the whole beam at each propagation position: this is a necessary condition for the soliton formation and consequently for diffraction compensation. The soliton solution (at least for the lowest soliton order) is, in fact, a pure amplitude solution, without any phase modulation across the beam (in case of breathing solitons, a transverse phase modulation is present in order to slightly focus and defocus the beam). This is analogous to saying that the angular momentum of the soliton beams with rotating polarization must be a constant of motion, as it was analytically considered as basic hypothesis for the soliton solution [6].

The light propagation in the homogeneous polarization regime is then represented on the Poincaré sphere, as shown in Fig. 8 where the S_1-S_2 projections of the sphere describe the polarization evolutions at increasing biases. For 0 kV/cm of external bias, the polarization dynamics describes an equatorial arc as large as about 310°. Already at 10 kV/cm, the polarization dynamics describes more than one complete turn around the sphere (a bit more than $\frac{7}{2}\pi$). By increasing the bias it is evident that the polarization rotation accelerates, describing many turns, but on the same time the induced birefringence pushes the polarization to follow smaller trajectories which approach the S_3 axis (at 35 kV/cm, the polarization trajectory passes for the circular state). Increasing more the external bias, the dynamics is more concentrated within the region for $S_1>0$, rotating around a stable state: actually, it is quite clear, observing all the obtained trajectories, that all of them rotate around a stable state, which is located within the plane $S_2=0$. Without bias, the center of the polarization rotation is $S_1=0$, while increasing the exter-

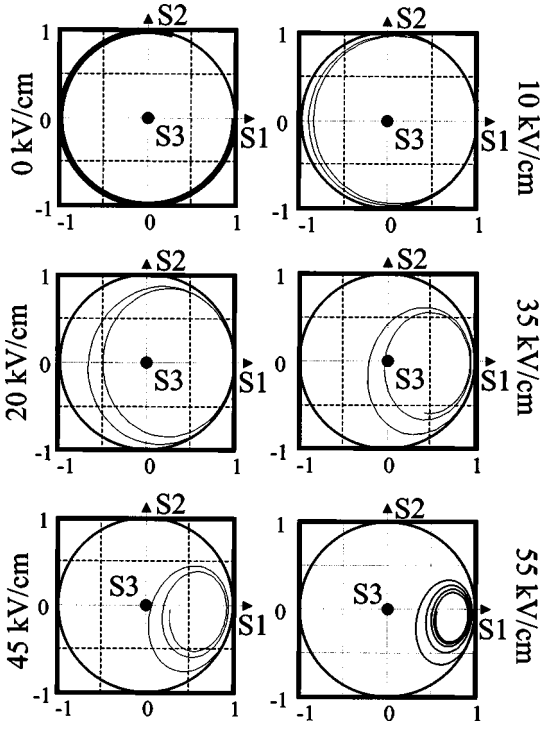

FIG. 8. Representation of the polarization dynamics of the beam for increasing applied biases. The graphics show the S_1-S_2 plane projection of the Poincaré sphere: we have chosen this planar representation of the sphere, instead of the whole 3D one, because it is the only representation able to show the whole polarization trajectories. By increasing the applied biases, the trajectories roll up in smaller and smaller loops. At 45 and 55 kV/cm, the trajectories are confined in the semiplane $S_1>0$, which means the polarization is not anymore completely rotating but vibrates around the *Y* direction. All the orbits converge towards an attractor state, which is an elliptic state, with the axis oriented as *X* and *Y*, and with ellipticity $\delta\varepsilon_{\mathrm{NL}}/\Gamma$.

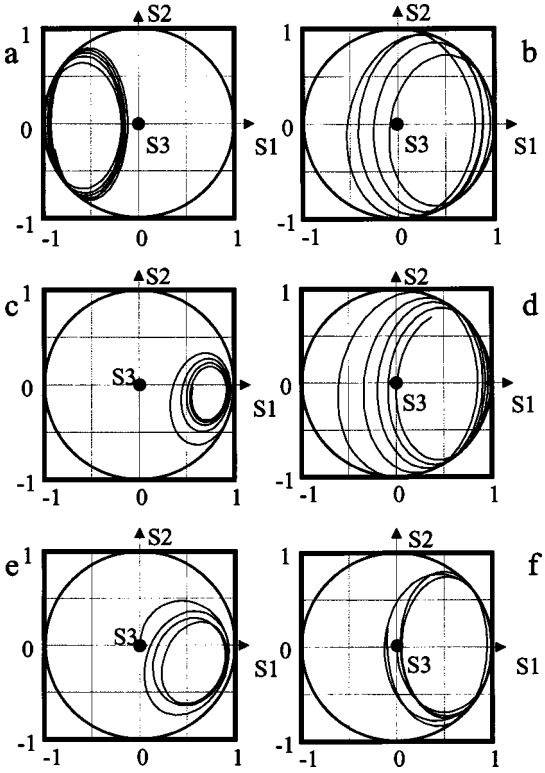

FIG. 9. Representation of the polarization dynamics of the beam at 55 kV/cm of applied bias for different input polarization states. (a) *X* polarization injected; (b) 45°-rotated polarization injected; (c) *Y* polarization injected; (d) 135°-rotated polarization injected; (e) circular polarization, rotating parallel to the optical activity axis; (f) circular polarization, rotating antiparallel to the optical activity axis.

nal bias the center of the polarization rotation moves towards the *Y* axis, i.e., forcing the polarization to follow rotation loops smaller and smaller around the attraction state defined by a dephasing of $\pi/2$ between polarizations (i.e., the major axis parallel to the *Y* direction) and by an ellipticity of $\delta\varepsilon_{\mathrm{NL}}/\Gamma$. It is clear from dynamical paths in Fig. 8 that the injected beam needs some propagation to follow in the final loop: this occurs, in our simulation, only for 45 and 55 kV/cm applied, whose final polarization states are described by loops almost overlapping after each round turn. In these regimes, the polarization is finally stable during propagation, homogeneous along the transverse direction, and the beam confined: thus, we can affirm that in these conditions a pure solitonic state is reached.

The initial polarization state is critical for the soliton formation, as previously described for the beam propagation. Thus, we have analyzed, always on the Poincaré sphere, the polarization dynamics from different polarization states, as shown in Fig. 9 (here the numbering follows the same numbering of Fig. 3 for easier comparison). Injecting a linear *X* polarization [case (a): initial state at $S_1=-1$, $S_2=0$, $S_3=0$,] the laser beam does not form any confined state but diverges; its polarization dynamics still describes an high acceleration of the rotation, which now occurs in an unstable region. The beam polarization is now following loops larger and larger because its light diffracts. Injecting a linear polarization at 45° [case (b): initial state at $S_1=0$, $S_2=1$, $S_3=0$], and 135° [case (d): initial state at $S_1=0$, $S_2=-1$, $S_3=0$] with respect to the *X* direction, the polarization follows large trajectories which are converging towards the attraction state (dephasing $\pi/2$, ellipticity $\delta\varepsilon/\Gamma$) located in the semiplane ($S_2=0$,$S_1>0$). Injecting a *Y*-polarized beam [case (c): initial state at $S_1=1$, $S_2=0$, $S_3=0$], the dynamic route is soon attracted in a stable loop, i.e., it forms a stable soliton. Injecting a circular polarization rotating in the same direction of the optical activity one [case (e): initial state at $S_1=0$, $S_2=0$, $S_3=1$; clockwise rotation] again the dynamic route is attracted in an almost stable loop, larger than the linear *Y*-polarization case. In fact from the intensity propagation map shown in Fig. 3(e), it is clear that the beam is still self-confined but is strongly pulsing around different dimensions (and polarization states). The final case is the injection of a circular polarization with an opposite rotation with respect to the optical activity [case (f): initial state at $S_1=0$, $S_2=0$, $S_3=1$; counterclockwise rotation]. The trajectory starts from the initial state and rotates (counterclockwise) towards the $S_1=1$, $S_2=0$, $S_3=0$ state (*Y* polarization): at this point the polarization rotation is inverted by the optical activity that dominates the dynamics, forcing the polarization

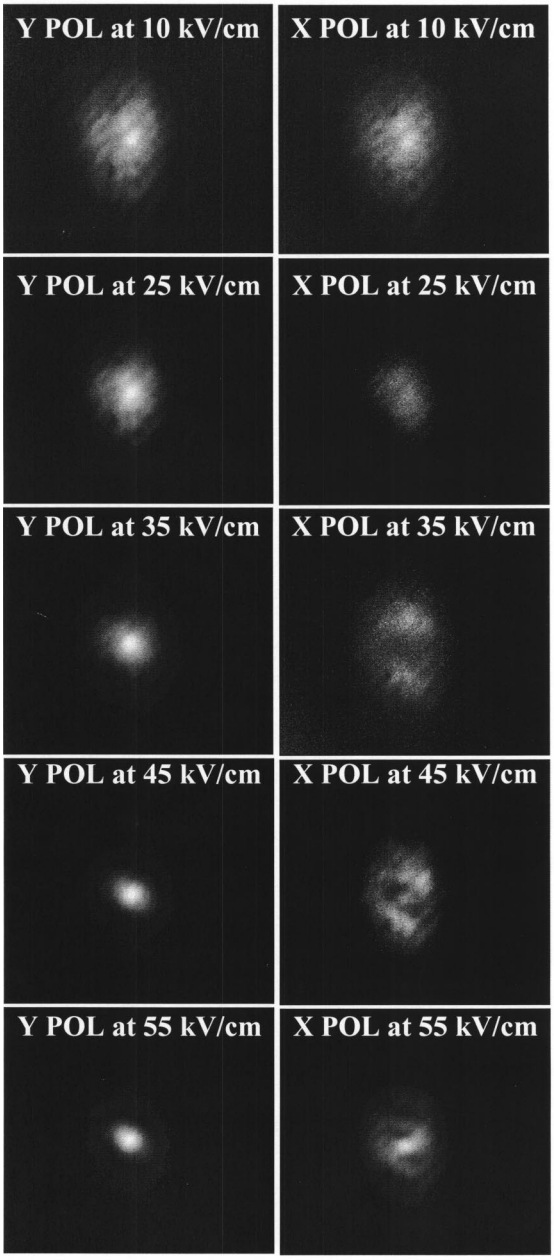

FIG. 10. Experimental images of the *X* and *Y* polarization components at the output plane for different applied bias. The large rings visible for the *X* component at 35 and 45 kV/cm are the losses given by the breathing because a Gaussian beam is injected at the input. It can be observed that these losses do not rotate but keep a fixed polarization, as numerically described in the maps of Fig. 7. At 55 kV/cm, the soliton is completely formed: along the two crossed polarization direction, the same profile is present because the solitonic polarization state is now elliptical.

to rotate again in the clockwise direction. As in the first case (a) diffraction dominates the intensity propagation, leading the polarization to follow larger and larger loops.

We have experimentally analyzed the polarization properties of the beam at the output plane recording the beam profiles for the *Y*- and *X*-polarization orientations at different bias fields, as shown in Fig. 10. At 10 kV/cm, the polarization state is almost linear and large. At 25 kV/cm, the beam is smaller and the polarization state shows that the *Y* profile is more intense than the *X* component. At 35 kV/cm, the *X* component is now larger with an darker hole inside: this behavior is clearly described by the polarization map in Fig. 7; the beam is going towards a solitonic profile losing some energy during propagation. This lost energy is located as rings around the beam (much brighter along the *Y* direction). The central part of the beam has now only an *Y*-polarization component: in fact, the central part of the *X* component is now dark. At 45 kV/cm, the beam has almost reached an elliptical state: in fact the confined beam has now both the *X* and *Y* polarization components. It is interesting to note that the diffracted portion of the beam (i.e., the large ring present is the *X*-polarization image) has a fixed polarization that does not rotate anymore, neither becomes elliptical. This feature was numerically found in the polarization maps of Fig. 7, where it is possible to follow these propagation losses without polarization rotation. At about 55 kV/cm, the polarization state is now described by both the *X* and *Y* components, both of them completely confined. Still, here small losses are present in the *X* component, whose intensity is much smaller than the solitonic beam. It must be pointed out here that the presence of losses does not mean that the solitonic beam is lossy while that the injected Gaussian profile is not optimized for the solitonic formation.

IV. COMPARISON WITH THE ANALYTICAL SOLUTION

Analytical solutions for the soliton formation in photorefractive materials with strong optical activity have been recently found [9] and experimentally verified for the (1+1)-dimensional case. The coupled equations (1) for the light propagation in photorefractive materials (in the slowly varying envelope approximation [5]), have been analytically solved, under the hypothesis of constant angular momentum of the spatial soliton during propagation. This assumption is the basis for the soliton formation as already described. It allowed to express the beam as the vectorial product of two fields, one transverse (describing the transverse shape of the beam) and one longitudinal along the propagation direction (describing the angular rotation of the polarization): this last longitudinal field is constant for the soliton. The constant-momentum assumption, using cylindrical coordinates normalized to the photorefractive nonlinearity ($Z=ckz$, $\phi=\arctan(y/x)$, $r=\sqrt{c}k\sqrt{x^2+y^2}$ or better $r_N \approx [\sqrt{\pi/2R}\cos(\frac{1}{2}\phi+\frac{1}{2}g_1 kz-\pi/4)]r$, where $c=n_0^2 r_{41}E_0$ and R is the intensity ratio $I_{\text{soliton}}/I_{\text{background}}$) gave the analytical solitonic solution

$$I(r,\varphi,Z)=\frac{2RI_{\text{background}}}{\pi^2 w_0^2}\gamma^2 e^{(2r_N^2/w_0^2)}\left[1+\frac{2}{\cosh^2(\sqrt{2}r_N)}\right], \tag{7}$$

where w_0 is the input Gaussian beam width and γ^2 is a normalized term which describes the periodical beam breathing. According to Eq. (7), the soliton width is

$$w_{\text{soliton}} = \frac{1}{k\sqrt{n_0^2 r_{41} E_0}} \left[\frac{\pi^2}{4R^2} + \frac{1}{w_0^2} \right]^{1/2}, \tag{8}$$

which means that it is scaling as $(w_0 R)^{-1}$, as expected. For our experimental case, considering $w_0 = 10.5\ \mu$m and $R = 4$, we obtain a necessary bias between 55 and 58 kV/cm in order to reach the soliton solution, which is in good agreement with the experimental observations.

V. CONCLUSIONS

In the conclusion, we have demonstrated experimentally that $(2+1)$-dimensional solitons are generated over 4.5 diffraction lengths of propagation in BSO crystals, a photorefractive material with large optical activity. The experimental solitonic state has been reached numerically by analyzing the dynamics of the soliton formation. We have found that it is influenced by an acceleration of the angular speed of light polarization (which prevents the beam from broadening by making the polarization rotation period much shorter than the diffraction length) and contemporarily by an induced birefringence. The soliton is formed where the induced birefringence becomes constant across the beam, and the polarization is trapped in a stable loop around an attraction state (which is described by an elliptical polarization, defined by a $\pi/2$ dephasing between X and Y components, which means with the major axis parallel to Y, and by an ellipticity $\delta\varepsilon_{\text{NL}}/\Gamma$). The numerical analysis of the soliton formation guided the experimental investigation, whose results are in good agreement with the previously proposed-analytical solutions for the soliton.

ACKNOWLEDGMENTS

The authors would like to acknowledge A. A. Kamshilin, A. V. Khomenko, and S. Odoulov for their useful and constructive advices. W.R. undertook this work with the support of the ''ICTP Program for Training and Research in Italian Laboratories,'' Trieste, Italy. E.F., A.P., and V.I.V. acknowledge the support of this collaborative work by the Project No. 36 of the Bilateral Collaboration Agreement in R&D between Italy and Romania, by the national CERES Project No. 136, as well as by ''Accademia di Romania'' in Roma.

[1] M. Segev, B. Crosignani, A. Yariv, and B. Fischer, Phys. Rev. Lett. **68**, 923 (1992).
[2] B. Crosignani, M. Segev, D. Engin, P. di Porto, A. Yariv, and G. J. Salamo, J. Opt. Soc. Am. B **10**, 446 (1993).
[3] E. DelRe, B. Crosignani, and P. di Porto, in *Spatial Solitons*, edited by S. Trillo and W. Tourellas, Springer Series in Optical Sciences Vol. 82 (Springer, Berlin, 2001).
[4] S. R. Singh and D. N. Christodoulidis, J. Opt. Soc. Am. B **13**, 719 (1996).
[5] W. Krolikowski, N. Akhmediev, D. R. Andersen, and B. Luther-Davies, Opt. Commun. **132**, 179 (1996).
[6] M. Segev, G. C. Valley, B. Crosignani, P. di Porto, and A. Yariv, Phys. Rev. Lett. **73**, 3211 (1994).
[7] M. P. Petrov, S. I. Stepanov, and A. V. Khomenko, in *Photorefractive Crystals in Coherent Optical Systems* (Springer-Verlag, Berlin, 1991).
[8] E. Fazio, F. Mariani, A. Funto, M. Zitelli, M. Bertolotti, V. Babin, and V. I. Vlad, J. Opt. A, Pure Appl. Opt. **3**, 466 (2001).
[9] E. Fazio, V. Babin, M. Bertolotti, and V. I. Vlad, Phys. Rev. E **66**, 016605 (2002).
[10] A. Marrakchi, R. V. Johnson, and A. R. Tanguay, Jr., J. Opt. Soc. Am. B **3**, 321 (1986).
[11] B. I. Sturman, E. V. Podivilov, V. P. Kamenov, E. Nippolainen, and A. A. Kamshilin, J. Exp. Theor. Phys. **92**, 108 (2001).
[12] B. Crosignani, M. Segev, D. Engin, P. di Porto, A. Yariv, and G. J. Salamo, J. Opt. Soc. Am. B **10**, 446 (1993).
[13] A. Zozulya and D. Anderson, Phys. Rev. A **51**, 1520 (1995).
[14] A. A. Zozulya, D. Z. Anderson, A. V. Mamaev, and M. Saffman, Europhys. Lett. **36**, 419 (1996).
[15] M. Born and E. Wolf, *Principles of Optics*, 6th ed. (Pergamon Oxford, NY, 1980).